

The Final Merger of Black-Hole Binaries

JOAN CENTRELLA¹, JOHN G. BAKER², BERNARD J. KELLY³, AND
JAMES R. VAN METER⁴

¹*Gravitational Astrophysics Laboratory, NASA GSFC, 8800 Greenbelt Rd.,
Greenbelt, MD 20771, USA*

email: Joan.M.Centrella@nasa.gov; corresponding author

²*Gravitational Astrophysics Laboratory, NASA GSFC, 8800 Greenbelt Rd.,
Greenbelt, MD 20771, USA*

email: John.G.Baker@nasa.gov

³*CRESST & Gravitational Astrophysics Laboratory, NASA/GSFC, 8800
Greenbelt Rd., Greenbelt, MD 20771, USA*

*Dept. of Physics, University of Maryland, Baltimore County, 1000 Hilltop
Circle, Baltimore, MD 21250, USA*

email: Bernard.J.Kelly@nasa.gov

⁴*CRESST & Gravitational Astrophysics Laboratory, NASA/GSFC, 8800
Greenbelt Rd., Greenbelt, MD 20771, USA*

*Dept. of Physics, University of Maryland, Baltimore County, 1000 Hilltop
Circle, Baltimore, MD 21250, USA*

email: James.R.VanMeter@nasa.gov

Key Words Black Holes, Gravitational Waves, Numerical Relativity

Abstract Recent breakthroughs in the field of numerical relativity have led to dramatic progress in understanding the predictions of General Relativity for the dynamical interactions of two black holes in the regime of very strong gravitational fields. Such black-hole binaries are important astrophysical systems and are a key target of current and developing gravitational-wave detectors. The waveform signature of strong gravitational radiation emitted as the black holes fall together and merge provides a clear observable record of the process. After decades of slow progress, these mergers and the gravitational-wave signals they generate can now be routinely calculated using the methods of numerical relativity. We review recent advances in understanding the predicted physics of events and the consequent radiation, and discuss some of the impacts this new knowledge is having in various areas of astrophysics.

CONTENTS

Introduction	3
Steps toward a robust black-hole binary model	6
<i>Overview of Numerical Relativity Issues</i>	6
<i>The Lazarus Approach: Hybrid Black Hole Merger Waveforms</i>	9
<i>Toward Evolving a Black-Hole Binary Orbit</i>	10
<i>Robust black-hole binary simulations</i>	12
The Physics of Black-Hole Binaries	14
<i>Merger Dynamics and Waveforms</i>	15
<i>The Spin of the Final Black Hole</i>	20
<i>Recoil Kicks from Gravitational Radiation</i>	21
<i>Longer Waveforms: Modeling the Late Inspiral</i>	23
Applications in Astrophysics	26
<i>Waveforms for Gravitational-Wave Observations</i>	27
<i>Consequences of Merger Recoil</i>	29
<i>Mass and Spin Evolution</i>	30

Outlook	31
<i>Complete Analytic Waveform Models</i>	31
<i>Improved Numerical Methods</i>	32
<i>Including Gas and Magnetic Fields</i>	34
Conclusion	35

1 Introduction

1.0.1 BLACK HOLES It has been nearly a century since Albert Einstein’s profound physical insight revealed our current standard model of gravitational physics, General Relativity. Among the theory’s extraordinary consequences was the predicted existence of black holes, nonlinearly self-gravitating, stable objects in which gravitational forces have completely overcome all other physical interactions. Though once considered a mathematical curiosity, General relativity’s description of black holes now provides the best explanation for a widespread class of astrophysical objects whose gravitational potential wells power many of the most energetic astronomical phenomena observed. These range from stellar black-holes powering X-ray sources in the neighboring regions of our galaxy, to supermassive monsters with masses $\sim (10^6 - 10^9)M_\odot$, where M_\odot is the mass of the Sun, with far-reaching astrophysical consequences.

1.0.2 GRAVITATIONAL WAVE OBSERVATIONS In the coming decade, anticipated observations of gravitational waves from black hole binaries will open a new window onto the universe. Interpreting such observations will richly engage aspects of our theoretical understanding of strong-field gravity which have never before been confronted with empirical observations.

The final coalescence of binaries consisting of two comparable-mass black-holes,

with mass ratios $q = M_1/M_2 \sim (1 - 10)$, is expected to be one of the strongest astrophysical sources of energy in the form of gravitational radiation. As the emission of gravitational waves removes energy and momentum from the binary, the orbits shrink and the black holes eventually merge together into a single black hole, producing an intense burst of radiation. With the advent of ground-based gravitational wave detectors such as LIGO and VIRGO (which will detect mergers of black holes with masses in the range $\sim (10 - 100)M_\odot$), and with planning underway for the space-based LISA (which will observe mergers of massive black holes, with masses $\sim (10^4 - 10^6)M_\odot$), knowledge of black-hole binary gravitational waveforms is urgent.

1.0.3 BLACK-HOLE BINARY COALESCENCE Black-hole binary coalescence can be thought of as proceeding in three stages. During the inspiral the holes have wide enough separations that they can be treated as point particles. In this stage, the orbital period is much shorter than the timescale on which the orbital parameters change, and the holes spiral together on quasi-circular orbits. When the holes get so close together that they can no longer be approximated as point particles, they enter the merger phase. In this strong-field, dynamical regime, the black holes plunge together and merge into a single, highly distorted black hole, surrounded by a common horizon. This remnant black hole then “rings down,” shedding its nonaxisymmetric modes through gravitational wave emission and settling down into a quiescent rotating black hole.

1.0.4 GRAVITATIONAL WAVES FROM THE COALESCENCE Knowledge of the gravitational waveforms from these three stages of black hole coalescence is important for gravitational wave detection and data analysis, as well as astrophysical applications. The inspiral can be calculated analytically using the post-

Newtonian (PN) approximation, which is an expansion of the full equations of General Relativity in powers of $\epsilon \sim v^2/c^2 \sim GM/(Rc^2)$, where v is the characteristic velocity of the source, M is its mass, and R is its characteristic size. The inspiral gravitational waveform is a “chirp”, which is a sinusoid increasing in both frequency and amplitude. The ringdown can also be calculated analytically using techniques of black-hole perturbation theory, and the resulting gravitational waveforms are damped sinusoids. However, the merger stage can only be understood using full numerical simulations of the Einstein equations in 3-D, and the resulting gravitational waveforms were unknown – until recently.

The final merger of comparable-mass black holes is a powerful source of gravitational radiation. The gravitational waveforms emitted by a black-hole binary with mass ratio q scale with the total mass M of the binary. Setting $c = 1$ and $G = 1$, we can express both length and time scales in terms of the total mass: $1M \sim 5 \times 10^{-6}(M/M_\odot)\text{sec} \sim 1.5(M/M_\odot)\text{km}$. The strong-field merger will produce a burst of gravitational radiation lasting $\sim 100M$ and having a luminosity $\sim 10^{23}L_\odot$, which is greater than the combined luminosities of all the stars in the visible universe. For stellar black-hole binaries ($M \sim 10M_\odot$) this luminosity will last for ~ 5 ms, and for massive black-hole binaries ($M \sim 10^6M_\odot$), for ~ 10 min.

1.0.5 CALCULATING THE MERGER Understanding the final merger of a black-hole binary requires solving the full Einstein equations using the methods of numerical relativity. This endeavor has proved to have many challenging aspects, ranging from providing astrophysically relevant initial data to understanding the structure of the Einstein equations, and the solution eluded researchers for many years. Recently, a series of dramatic breakthroughs has ignited the field, making robust, stable, and accurate simulations of binary mergers possible for the

first time. These models are opening our understanding of strong-field dynamics, impacting gravitational wave searches and other areas of astrophysics. In this article we provide an overview of these exciting developments, highlighting the key physical results that are emerging.

2 Steps toward a robust black-hole binary model

Computing the strong-field merger of two comparable-mass black holes has a long history, with the first attempt dating back more than 40 years. Overall, progress was generally slow and incremental, requiring the interplay among new ideas in black hole modeling, mathematical investigations into the structure of the Einstein equations, the development of effective gauge conditions, advances in computational techniques, and the availability of high performance computing resources. Here we provide a brief review of key developments in this arena.

2.1 Overview of Numerical Relativity Issues

Solving Einstein's equations on a computer typically requires slicing 4-D space-time into a stack of 3-D spacelike hypersurfaces, each labeled by time t (1, 2, 3). The Einstein equations then divide into two sets: constraint and evolution equations. The constraints are a set of time-independent elliptical equations that must hold on each slice. In particular, the constraints are solved first to obtain valid initial data for a black-hole binary simulation. This data is then propagated forward in time using the evolution equations.

2.1.1 GAUGE FREEDOM General Relativity has four spacetime coordinate degrees of freedom, which are associated with four freely-specifiable coordinate or gauge functions that govern the future development of both time and the spatial

coordinates. These are generally taken to be the lapse function α , which gives the lapse of proper time ($\alpha \delta t$) between neighboring slices, and the shift vector β^i , which determines how the spatial coordinates develop from one slice to the next. Appropriate choices for the lapse and shift have proven to be crucial for successful black hole evolutions (4,5).

2.1.2 FORMULATION OF THE EVOLUTION EQUATIONS For many years, a primary challenge of numerical relativity was simply to decide which equations to solve (3). There is no unique formulation of the Einstein equations; rather there are many choices regarding, for example, which variables to use, whether to write the equations as first-order or second-order in time, and which coordinate conditions to impose. These choices are not arbitrary because some formulations turn out to be more “numerically friendly” than others. That is, although they are analytically equivalent when constraints and auxiliary variable definitions are assumed exact, some formulations may be unstable in practice. For example, the evolution equations may admit rapidly growing solutions which violate the constraints. In this case, although the initial data may contain only tiny errors, the subsequent evolution may produce violations of Einstein’s equations which “blow-up”. There can also be pathological numerical solutions that don’t represent solutions to the analytic evolution equations at all, but are supported by the discrete numerical grid structure and depend on the details of the finite-differencing operators.

2.1.3 NUMERICAL METHODS Once a formulation has been chosen, the Einstein equations are solved numerically for various field variables on a grid of discrete points that represents the spacetime domain of interest. There are two general approaches for dealing with the spatial derivatives that appear in these

equations. Finite differencing interpolates the derivative at a given point from the surrounding points according to a Taylor expansion in the grid spacing. Spectral methods assume a solution in the form of a summation of orthogonal functions; once the coefficients are obtained numerically, the derivatives can be found analytically. In both cases, time integration can be handled in a number of ways, most commonly by a Runge-Kutta algorithm. To date, most numerical relativity solutions have been carried out using finite differencing, with most current work employing a Cartesian grid in three spatial dimensions, although results from evolutions using spectral methods are now becoming available.

2.1.4 INITIAL CONDITIONS FOR BLACK HOLES To model astrophysical binaries, initial data must be generated for two black holes moving on quasicircular inspiralling orbits and having a mass-ratio q and some configuration of spins. One usually conceptualizes the initial state of the system with a particle-like description of the masses, positions, momenta, and spins of each black hole. Since general relativity is a field theory, such a description can only be seen as a first step. The model requires a full description for the initial field configuration which satisfies General Relativity's four initial value constraints, and which somehow corresponds to the system we have described in these particle-like terms.

2.1.5 EVOLVING THE BINARY This system is evolved for several orbits and then through plunge, merger, and ringdown, for a total duration on the order of several hundred M or more. To obtain the gravitational waveforms, the radiation must be extracted from the simulation at large enough distances from the source to be in the “wave zone”. Since the length scales of the black holes are $\sim M$ and the wavelengths of the emitted radiation are $\sim (10 - 100)M$, it is clear that some sort of variable resolution such as adaptive mesh refinement must be used

to handle the very large computational domains needed.

2.2 The Lazarus Approach: Hybrid Black Hole Merger Waveforms

By the late 1990's numerical relativity had developed to the point that brief simulations of black-hole binaries in three spatial dimensions plus time were possible. These techniques were sufficient for evolving promptly merging “grazing collisions” of black holes (6,7). However, the simulations were not indefinitely stable, but rather would typically crash after $\sim (10 - 30)M$, well before any significant portion of a binary orbit could be evolved.

2.2.1 HYBRID SIMULATIONS In this arena, the Lazarus method emerged as a novel approach to obtaining black-hole binary waveforms, combining short numerical relativity simulations with black hole perturbation methods (8). Since numerical relativity codes were then only able to evolve for a brief period, and since perturbation theory could approximate the late time dynamics of the distorted remnant black hole, the Lazarus Project aimed to apply numerical relativity to evolve the strong-field approach to merger, thereby providing a hybrid model for a significant part of the problem. Starting from quasi-circular initial configurations near the start of the final merger, the black holes were evolved using numerical relativity for $\sim 15M$ until just before the simulation became inaccurate. Then, via a complicated interface, data from late in the numerical simulations was interpreted as initial data describing the perturbed final black hole and the emerging radiation. Finally, black hole perturbation theory techniques were applied to evolve this data and derive the full waveforms.

2.2.2 FIRST RESULTS The Lazarus simulations gave the first indication of what might be expected for the terminal burst of radiation from coalescing black-hole binaries. Figure 1 shows that the dominant $\ell = 2, m = 2$ spin-(-2)-weighted spherical harmonic component has a brief burst of radiation smoothly joining the damped sinusoidal signal of the ringdown. The waveforms were remarkable for their simplicity, with predominantly circular polarization (in the $\ell = 2, m = 2$ mode), and a steady evolution of polarization frequency and amplitude. Since these characteristics were robust under variations in the model, it was conjectured that the waveforms from a binary starting from a wide separation late in the inspiral would be well characterized by these simple features. Subsequently, the Lazarus method was applied to study mergers of more generic black-hole binaries (10, 11).

2.3 Toward Evolving a Black-Hole Binary Orbit

2.3.1 THE BSSN SYSTEM Concurrently with the Lazarus investigations, further progress was being made toward full numerical relativity simulations of black-hole binary mergers. One major milestone was the development of a conformal formulation of the Einstein equations known as the Baumgarte-Shapiro-Shibata-Nakamura or “BSSN” system (12), that overcame some instability problems associated with an earlier formulation in use at the time (1, 13). In this approach, the set of evolution equations is written with first-order time derivatives and second-order spatial derivatives, and is strongly hyperbolic (14). Stable time evolution was accomplished using a coordinate condition that evolves the lapse function dynamically, causing the slices to avoid crashing into the black hole singularities (15, 7). However the simulations were still limited to durations

$\lesssim (30 - 40)M$ of stable evolution, by a failure of the spatial coordinate system known as “grid stretching,” in which the coordinates tend to fall into the black holes, and by instabilities related to how the black holes were handled numerically.

2.3.2 CONTROLLING THE SPATIAL COORDINATES Eliminating grid-stretching required developing appropriate techniques for dynamically controlling the spatial coordinates, which are governed by the evolution of the shift vector. The first long-lasting evolutions of distorted black holes relied on a class of hyperbolic shift evolution schemes, known as Γ -freezing conditions, which were inspired by the BSSN formulation. With this approach, a single distorted black hole could be evolved indefinitely (e.g., for thousands of M) with reasonable accuracy (16). These studies allowed the full numerical determination of gravitational waveforms from black hole ringdowns as the distorted black hole settled down to a physically and numerically stable final state, and provided a foundation for future advances in black-hole binary simulations (5).

2.3.3 PROBLEMS WITH MOVING BLACK HOLES However, another aspect of spatial gauge conditions remained a critical issue for long-lasting black-hole binary simulations. As general relativity allows arbitrary coordinate systems, many groups adopted coordinate conditions which did not allow the black holes to move through the computational domain. This simplified the problem of dealing with the black hole singularities, which were handled either by excising the black hole interiors (within the horizons) from the computational domain (17), or by representing the black holes as punctures (18). Though progress had been made toward implementing moving excision regions (19), it was computationally much simpler to demand that the excision region remain fixed on the grid (20). Similarly, the puncture treatment was formulated so that the black hole was fixed

on the grid and the singularity was factored out and handled analytically in a time-independent manner. However, for binary configurations in which the black holes physically move, the cost of keeping the black holes fixed in coordinate space was paid by the twisting and stretching of the dynamical fields, eventually leading to large computational errors.

For inspiraling binary configurations one potential solution was to attempt to untwist the geometric field data by imposing comoving coordinates using a shift vector that is dynamically adjusted during the evolution of the binary to minimize motion of the black hole horizons (21). With this approach, Brügmann et al. achieved a significant milestone: the first simulation of a full orbital cycle of a black-hole binary system prior to merger (22). In this work, the authors applied a dynamically adjusted corotating frame tracking the measured position of the black hole apparent horizons. This allowed a simulation which remained accurate for a little longer than the $\gtrsim 100M$ duration of a complete orbit. However, problems occurred with the large characteristic speeds that resulted near the outer boundaries, limiting the domains of these simulations and preventing gravitational waveforms from being measured effectively. The coordinate control also required fine tuning which eventually failed, causing the simulation to crash as the black holes finally approached merger.

2.4 Robust black-hole binary simulations

2.4.1 FIRST ORBIT AND MERGER SIMULATION In early 2005 Pretorius shocked the numerical relativity community by announcing the first complete, robust simulations of an equal-mass black hole merger (23). After completing ~ 1 orbit, the black holes plunged and merged to form a single distorted black

hole that then rings down. Pretorius extracted the gravitational waves to obtain the first inspiraling merger waveform directly from numerical relativity, shown in Fig. 2.

Pretorius employed several techniques that were very different from most other numerical approaches to the black-hole binary problem (24). Rather than using the BSSN formulation, he applied a generalized harmonic formalism (25), directly integrating the spacetime metric with evolution equations of second-order in both space and time. These equations were implemented numerically using adaptive mesh refinement to allow high resolution around the black holes while maintaining a large computational domain. Pretorius utilized spatial coordinates compactified to draw spatial infinity into the computational domain, with a choice of gauge-evolution strongly tied to his evolution formalism. Following (26), he added terms to the evolution equations to specifically damp away any violations of the constraints. In his simulations, the black holes were excised and moved freely across the computational grid. Pretorius’ success with such novel methods quickly raised questions as to whether the struggling, more widely-pursued BSSN-based puncture approach might be off course.

2.4.2 MOVING PUNCTURES Later that same year, however, a new robust method based on the BSSN formulation was announced. The “moving puncture” method was discovered simultaneously and independently by the groups at the University of Texas at Brownsville (UTB) (27) and NASA’s Goddard Space Flight Center (GSFC) (28). In this approach the black holes are represented as punctures, but are not constrained to remain fixed on the coordinate grid. Rather, they are allowed to move freely through the grid using novel coordinate conditions. Figure 3 shows the trajectories of the puncture black holes as com-

puted by the UTB group; the formation of a common horizon marks the point of merger. The moving puncture method eliminates the analytic representation of the puncture singularities in favor of an approximate numerical treatment within the black hole horizons.

The UTB and GSFC groups had discovered and applied similar methods to the same problem: evolving an equal-mass nonspinning black-hole binary from near the final orbit, through merger and ringdown, and studying the gravitational waves. The first generation of merger waveforms from Pretorius, GSFC, and UTB showed the same simple burst of radiation ending in a damped-sinusoidal ringdown, and were qualitatively consistent with the Lazarus project results discussed above and shown in Fig. 1.

The discovery of the moving puncture method ignited the field of black-hole binary evolutions. Since it was based on commonly used methods, most researchers in the field were quickly able to achieve accurate and stable evolutions using their existing codes, with the adoption of simple coordinate conditions (29). Suddenly, the game was on and nearly all the groups were participating.

3 The Physics of Black-Hole Binaries

With the advent of successful numerical evolutions of binaries that inspiral and merge, the numerical relativity community's focus changed to investigating the physics of binary mergers. This advancing frontier is enabled by continued technical improvements in areas ranging from initial data prescriptions to more accurate numerical methods.

3.1 Merger Dynamics and Waveforms

The astrophysical black hole mergers that are the targets of current and future gravitational wave detectors are expected to reach the merger stage after having radiated away any initial eccentricity (30) and proceeding through a long quasi-circular inspiral. All equal-mass, nonspinning binary merger simulations starting from such orbits in the inspiral should produce the same gravitational waveform, subject only to rescaling with the total mass of the system. For many years, concerns had been raised about the accuracy and realism of black-hole binary initial data sets, including the effects of spurious gravitational radiation and eccentricity (31,32,33). With numerical relativity now able to simulate the final merger, the next step was to run models with enough orbits before the plunge and merger to get complete and reproducible waveforms starting from the late inspiral.

3.1.1 EQUAL-MASS, NONSPINNING BLACK HOLES The GSFC group produced the first representation of the definitive waveform for the final stages of a merger of equal-mass, nonspinning black holes (34). They carried out a series of four simulations with the holes starting from quasicircular initial conditions at increasingly larger separations. In these runs, the holes completed $\sim 1.8, 2.5, 3.6$, and 4.2 orbits before the formation of a common horizon. To compare the results of these models, they chose the moment of peak gravitational radiation amplitude as the fiducial time $t = 0$.

The orbital dynamics of the binaries can be examined by tracking the black hole centers, given by the location of the punctures. The black hole trajectories for each run were oriented so that they superpose at the fiducial $t = 0$. In the early stages of each run, the tracks clearly showed the effects of eccentricity in

the initial conditions, with the amount of initial eccentricity decreasing for more widely separated holes. As the holes spiraled together deeper into the strong-field regime, the tracks locked on to a universal trajectory independent of their initial conditions that continued for the last orbit, plunge, and merger.

Figure 4 reveals the corresponding universal gravitational waveform. Here, the dominant $\ell = 2$, $m = 2$ quadrupolar component for each run is shown, shifted in time so that the peak radiation amplitude occurs at $t = 0$. Starting from $t = -50M$ the waveforms show nearly perfect agreement, differing from each other at the level of 1%. The signals for the preceding few orbits agree at the level of $\sim 10\%$, except for a brief burst of spurious radiation at the start of each run.

Note that the merger waveform shows a remarkably simple shape, making a smooth transition from the inspiral chirp to the damped sinusoid of the ring-down. As the merger begins, both the wave amplitude and frequency increase, albeit faster than in the inspiral. The amplitude reaches a peak and then decreases, dropping exponentially through the ringdown. The frequency increases monotonically to a maximum value that remains constant during the ringdown.

Of course, the black-hole binary merger dynamics and waveforms can be altered by the presence of large amounts of eccentricity (35) and spurious gravitational radiation (36) near the time of the plunge. However, the robustness of the merger to modest deviations from astrophysical initial conditions opened the door to studying many cases of interest using relatively short simulations, starting just a few orbits before the start of the plunge.

3.1.2 UNEQUAL-MASS, NONSPINNING BLACK HOLES Astrophysical black-hole binaries are unlikely to have exactly equal masses. Currently, numerical

relativists are able to evolve systems with mass ratios up to $q = 10$ (37). Starting from quasicircular orbits the simulations show that the merger phase for non-spinning, unequal mass black hole binaries is robust to modest deviations from these initial conditions and produces a generally simple waveform shape.

An important tool for analyzing these mergers is a decomposition into spin-weighted spherical harmonic modes. Berti et al. (38) analyzed a set of unequal-mass nonspinning mergers with mass ratios ranging from $q = 1$ to $q = 4$. Studying the multipolar distribution of the radiation, they found that the sub-dominant modes ($\ell > 2$) become more important, carrying a larger fraction of the energy, as q increases. Specifically, for $q > 2$, the $\ell = 3$ mode typically carries $\sim 10\%$ of the radiated energy. Also, as expected from symmetry considerations, the odd- m modes are suppressed in the equal-mass limit.

Baker et al. (39) carried out a complementary study of the radiation from nonspinning mergers with mass ratios in the range $1 \leq q \leq 6$. The multipolar decomposition clearly shows that the hallmark simplicity of the waveform persists for $q > 1$ and extends to each of the spherical harmonic components $\ell \geq 2$; this property has recently been shown to extend to the $q = 10$ case (37). In the full mode-summed waveform, this simple shape is also seen when viewing along the system's orbital axis, where the quadrupole mode dominates. A somewhat more complex appearance arises by viewing the system off-axis, where higher multipoles contribute more strongly to the waveform at various angles.

Throughout the entire coalescence, each of the spherical harmonic waveform components is circularly polarized, with steadily varying phase and amplitude (39). For each mass ratio q , the rotational phase (and frequency) of the different (ℓ, m) components are the same. During the inspiral this is expected, since the

waveform phase is equal to the rotational phase multiplied by the mode number m . However, for the $\ell = m$ modes this relationship also holds throughout the merger and into the ringdown.

These properties suggest a simple conceptual interpretation in which the radiation is generated by an “implicit rotating source.” In this picture, each (ℓ, m) mode is generated separately by the (ℓ, m) moment of some implicit source. The fixed relationship for the $\ell = m$ modes implies that these components of the source rotate rigidly through the entire coalescence. The $\ell \neq m$ components are less rigid and peel away from the main $\ell = m$ trend during the merger (39).

3.1.3 MERGERS OF BLACK HOLES WITH SPIN The mass ratio q is a one-dimensional cut into the parameter space of black-hole binaries. The remaining parameter space is dominated by the spin angular momentum of each hole. As spin is a vector quantity, this adds six more dimensions. Simulations of spinning black holes first focused on systems whose spins were expected, on the basis of PN arguments, to have the least effect on the orbital motion. Binaries with aligned and anti-aligned spins are relatively easy to treat as there is no precession of the orbital plane or the individual spins. When one or both holes has a spin not parallel to the orbital axis, spin-orbit and spin-spin interactions will cause precession that can complicate the evolution and the resulting waveforms (40).

The first merger evolutions of spinning black holes were carried out by Campanelli et al. (41). They simulated the mergers of two equal-mass highly spinning black holes with $(a/M)_{1,2} = .757$, and both spin vectors either aligned or anti-aligned with the orbital angular momentum. Here, $a \leq M$ is the magnitude of the black hole spin angular momentum per unit mass. They also evolved a nonspinning equal-mass binary for comparison. All three binaries had the same

initial orbital angular frequency corresponding to an orbital period $\sim 125M$, and merged to form a rotating remnant black hole with $(a/M)_{\text{final}} < 1$. However, the aligned system took noticeably more orbits to merge than the others. This behavior is caused by the spin-orbit interaction, which produces an effective force between the black holes, either an attractive or repulsive for the anti-aligned or aligned cases, respectively. All three binaries generate remarkably similar gravitational waveforms having a simple shape, with the aligned case displaying a longer wavetrain and the anti-aligned case a shorter one.

The first fully numerical evolutions of strongly precessing spinning systems were carried out by Campanelli et al. (42, 43), who observed both significant precession of the orbits and a “spin flip,” in which the final post-merger black hole spins in the direction opposite to the two initial black holes. More recent work is beginning to probe the effects of spin precession on waveforms (44).

Studies of this most general of (non-eccentric) parameter sets are still in the early stages. No systematic study of waveform shapes and polarizations has been carried out yet. A preliminary study of the multipolar structure of gravitational waves from several classes of binaries with equal spins has been performed by Berti et al. (45). They considered an equal-mass case with aligned spins; several $q = 4$ binaries with antialigned (down-down) spins; and three unequal-mass binaries with spins initially in the orbital plane and pointing in opposite directions. Examining the distribution of gravitational-wave energy emitted by various modes, they find that, as in the case of nonspinning mergers, odd- ℓ multipoles are suppressed for $q = 1$ and that, as q increases, more energy is radiated in higher- ℓ multipoles.

3.2 The Spin of the Final Black Hole

Because the state of the final black hole formed from the coalescence depends primarily on termination of the inspiral and the late burst of radiation in the merger, it can be accurately probed with relatively short simulations of just a few orbits.

The merger of two equal-mass nonspinning black holes produces a final black hole with a moderately high spin, $(a/M)_{\text{final}} \sim 0.69$ (9, 23, 27, 28, 46). Since the black holes each start out with no spin, and any tidal spin-up is negligible (47), the spin of this final black hole arises from the orbital angular momentum of the original binary. Simulations show that, for this simplest black hole merger, the final spin is “universal,” or independent of the initial black hole separation, for modest deviations from quasicircular initial conditions.

For mergers of nonspinning black holes with unequal masses, the spin of the final black hole decreases as the mass ratio q increases. Simulations with mass ratios up to $q = 10$ show that the final spin parameter scales as $(a/M)_{\text{final}} \sim q/(1+q)^2$, where $(a/M)_{\text{final}} \approx 0.48$ for $q = 4$ and $(a/M)_{\text{final}} \approx 0.26$ for $q = 10$ (38, 39, 37).

The effects of spin-orbit and spin-spin coupling can become important in determining the spin of the final black hole. In the simplest cases, the spin vectors are parallel to the orbital angular momentum. Depending on the mass ratio and the black hole spin, the merger can result in a final black hole with a larger (spun up) or a smaller (spun down) spin than either of the progenitors (10, 41, 48). In certain cases, the merger can lead to a spin flip with the final black hole spinning in a direction opposite to the spins of the initial holes; in particular, it is possible to produce a final nonspinning black hole, $(a/M)_{\text{final}} = 0$, from the merger of two

spinning holes (49, 45). More general black-hole binaries, with misaligned spins, are further complicated with the effects of precession (42, 50, 51).

Several attempts have been made to produce expressions for the final spin vector using analytic techniques or by fitting to results from numerical simulations (49, 52, 53); see (54) for a review. Of particular interest is the question of whether a black hole merger can produce a maximally spinning hole ($(a/M)_{\text{final}} = 1$) or indeed exceed the Kerr limit ($(a/M)_{\text{final}} > 1$). Current research suggests that this is not possible, even for mergers occurring from hyperbolic encounters (55) and mergers of highly boosted black holes (56).

3.3 Recoil Kicks from Gravitational Radiation

A notable phenomenon arising from asymmetric binary systems is the merger recoil or kick – a net movement of the end-state black hole from the system’s center of mass, caused by the anisotropic emission of gravitational radiation during the coalescence. Fitchett (57) produced a useful formula for the kick velocity, which has significant applications in astrophysics, using a quasi-Newtonian approximation. Several authors also calculated the recoil analytically using PN approximations (58). However, since the dominant part of the effect builds up in the strong-field regime close to merger, full numerical relativity simulations are needed for accurate calculations of the kick.

3.3.1 KICKS FROM NONSPINNING BLACK HOLE MERGERS In 2006, recoil from a fully numerical binary merger was demonstrated for the first time by Herrmann et al. (59), for plunging black-hole binaries with mass ratios as large as $q \sim 3.1$. This was followed soon afterwards by a full orbit and plunge simulation by Baker et al. (60), who found a recoil of between 86 and 97 kms^{-1} for a mass

ratio $q = 1.5$.

A more systematic study of recoil from mergers of unequal-mass binaries was produced by Gonzalez et al. in 2007 (61), who studied the merger of binary systems with mass ratios between $q = 1$ and $q = 4$. Figure 5 shows the resulting range of recoil speeds, together with several earlier numerical and analytical estimates. The authors synthesized these into a single recoil formula, a nonlinear correction to the Fitchett formula, yielding a maximum recoil of 175 kms^{-1} for a mass ratio of $q \sim 3$. This has recently been tested for the more extreme $q = 10$ mass ratio, with general agreement (37).

3.3.2 SPINNING BLACK HOLE MERGERS AND SUPERKICKS Calculations of recoil in the much larger parameter space of spinning binaries began with the non-precessing cases of holes with spins aligned (or anti-aligned) with the orbital angular momentum. Several studies of this region of parameter space (62,48) have revealed that the kick velocity has a quadratic dependence on initial spins, with a maximum kick of 448 kms^{-1} for extremal Kerr holes, $(a/M)_{1,2} = 1$. For these anti/aligned cases, as well as for nonspinning unequal-mass black-hole mergers, the direction of the kick velocity is always in the orbital plane.

Meanwhile attention turned to more general black hole spins. Campanelli et al. (43) speculated from PN arguments that optimal spin configurations could give rise to huge “superkicks,” with velocities $> 1000 \text{ kms}^{-1}$, out of the initial orbital plane. The first such superkick — around 2500 kms^{-1} — was soon observed by Gonzalez et al. (63). Tichy et al. (50) have argued that superkicks arise in mergers with general spin orientations, while greater insight into the mechanism of these kicks has been developed (64,65).

With such a large parameter space to cover, it seems useful to try to construct a

general formula that will describe kicks from arbitrarily spinning binaries. Baker et al. (66) used new and existing aligned-spin results to produce a single unifying formula for in-plane kicks; Campanelli et al. (43, 67) proposed an extension to this model, with scaling of the superkick out-of-plane contribution motivated by PN theory. The leading dependence in this formula on the angles between spins and linear momenta of the pre-merger holes has strong support from numerical simulations (67, 64, 68); however, the dominant scaling with mass ratio is still in dispute (69, 70).

3.4 Longer Waveforms: Modeling the Late Inspiral

Many key features of black-hole binary interactions can be modeled usefully with only a small handful of binary orbits before merger. Quantities such as radiated energy and momentum are bulked near the merger and have been shown to be robust to the addition of one or two extra orbits (see Section 3.1.1). However, optimal observational studies of gravitational waveforms ultimately require theoretical predictions for the full waveform, starting at large separations during the inspiral.

Before the breakthroughs in numerical relativity, most information about the dynamics of compact binaries came from PN theory. This approach supplied the particle trajectories, energy flux, and – most importantly for detector scientists – the gravitational waveforms themselves. However PN theory fails before the system merges, so the waveforms are necessarily incomplete. With the advent of numerical simulations encompassing many orbits, scientists finally have a way to develop complete information about the waveforms. This requires longer simulations which reveal the last part of the binary inspiral, and allow overlap with PN

waveform predictions.

3.4.1 LOW-ECCENTRICITY INITIAL DATA Simulations for these studies require careful attention to the initial configuration of the black holes. For a significant population of astrophysical binaries, it can be expected that the orbits have circularized through gravitational-wave emission over many orbits prior to merger. Numerical simulations try to mirror this expectation by selecting initial momenta consistent with near-zero eccentricity for the relatively small separations at which a full numerical relativity simulation becomes feasible.

For equal-mass, nonspinning binaries, two basic approaches have proved effective in reducing spurious eccentricity. The more direct method is to model the observed eccentricity, and then adjust the momenta using a Newton-like step to zero it out; this approach has led to extremely low eccentricities (71, 46). An alternative approach, adopted by Husa et al. (72), is to use the PN Hamiltonian equations of motion to model the early evolution of the particle trajectories, starting from large ($\sim 50 - 100M$) separations; the emission of radiation during this process naturally circularizes the orbit, and low-eccentricity momenta can be read off at the desired separation. This approach has recently been tested with spinning binaries as well (44).

The first long waveform was produced by the GSFC group (73, 74) for equal-mass, nonspinning black holes starting ~ 7 orbits or ~ 14 gravitational wave cycles before merger. Baker et al. estimated their numerical errors in waveform phase from (74) as a function of frequency, finding that above a certain frequency numerical errors are smaller than internal errors in the PN sequence. In addition, the numerical and PN waveform phases agree to within one radian of phase drift for a little over ten gravitational wave cycles preceding the last orbit before

merger, comparable to numerical error estimates. Hannam et al. (75) improved on this work, with phase and amplitude comparison between their low-eccentricity higher-resolution evolutions and PN waveforms.

3.4.2 EVOLUTIONS WITH SPECTRAL TECHNIQUES Numerical simulation codes based on pseudospectral differencing techniques are particularly well-suited to long waveform studies. The Caltech-Cornell group adopted the constraint-damped generalized harmonic formalism used by Pretorius, an important component in developing a stable spectral evolution code (76). Also like Pretorius, their code handles black holes by excising the black hole interiors. Their spectral code also employs a numerical grid that tracks the black holes explicitly. Though there can be difficulties with the changing geometry as black holes merge, this approach allows efficient study of the long-lasting inspiral waveforms.

Recently this approach has provided, several of the longest and most accurate black-hole binary evolutions.(46,77) In particular, the Caltech-Cornell group have used their spectral code to simulate an equal-mass nonspinning binary starting 16 orbits and 32 gravitational wave cycles before merger: see Fig. 6 (46) These much longer waveforms have been used to validate several competing PN models (71).

3.4.3 COMPARING RESULTS With so many pre-merger waveform cycles now available for the equal-mass case, the results can be cross-checked by comparing the “complete” waveform – inspiral, merger and ringdown – between groups. This is important to verify expectations that differences in methodology and residual numerical effects, such as unwanted eccentricity, are unimportant. A recent effort, dubbed the “Samurai project,” analyzed long waveforms from several groups in the light of detectability criteria for the LIGO and Virgo ground-based

gravitational-wave detectors. They found that the available numerical relativity waveforms are indistinguishable in these detectors for signal-to-noise ratios (SNRs) $\lesssim 25$ (78).

3.4.4 LONG WAVEFORMS FOR MORE GENERAL BLACK HOLES Hannam et al. have investigated the properties of highly spinning orbit-aligned black holes, comparing their phase and amplitude with PN predictions over the last ten waveform cycles (79). In the best cases, they find phase agreement within 2.5 rad for 3.5PN, and amplitude agreement to within around 12% with restricted PN. While not at the same level as their nonspinning results (75), this may be attributable to the lower orders of accuracy available for spinning black holes in PN theory at the present. The Caltech-Cornell group has recently conducted long-lasting simulations of black holes with spins aligned and anti-aligned with the orbital angular momentum, calibrating a tunable PN waveform model to match the results (77,80); see Sec. 5.1.

Generic mergers involving non-aligned, and thus precessing, spins adds four new degrees of freedom to the problem. A systematic understanding of waveforms generated by generic mergers will require considerably more study. Recent simulations have begun to explore generic examples (44).

4 Applications in Astrophysics

We have described a sampling of the explosion of numerical relativity studies revealing some of the details of black-hole binary physics as implied by General Relativity. While more remains to be learned, this new understanding is already making important contributions in planning and interpreting astrophysical black hole observations where Einstein's theory is applied as the standard model of

gravitational physics.

4.1 Waveforms for Gravitational-Wave Observations

Experimental gravitational-wave detectors were first developed more than 40 years ago. Although advances in design have increased their sensitivity by many orders of magnitude, the extreme weakness of expected astrophysical signals (strain amplitudes $\delta L/L \sim 10^{-21}$) means the observational challenge is still huge.

The output of any gravitational wave detector will be a data stream that must be combed through to find real signals. This search requires accurate “template” waveforms representing our best picture of the radiation from expected sources; these templates can then be compared with the data stream through matched filtering. We refer the reader to a review on gravitational-wave astronomy for an overview of these techniques (81).

Crucially, the most important sources of gravitational radiation are expected to include the mergers of black-hole binaries. Before the advent of numerical relativity simulations of black hole mergers, the only test waveforms available for use in data analysis studies were based on PN theory. These waveforms were essentially only inspiral chirps and did not include the strong-field merger. The new, richer, information now available from numerical relativity has revolutionized the data analysis picture in several ways.

4.1.1 DETECTING BLACK-HOLE MERGERS The availability of the plunge-merger-ringdown portion of the signal can greatly increase the SNR in the detector. Armed with a long numerical merger waveform of acceptable accuracy, we can extend it backwards to cover an arbitrarily long inspiral by matching to a PN waveform. Such a “hybrid” waveform was first produced by the GSFC group

for the equal-mass, nonspinning case (74). Using this hybrid, we can investigate the total achievable SNR, and the related distance reach, for current and future detectors. Figure 7 demonstrates the gain in SNR from including the merger portion of the waveform for the ground-based Advanced LIGO detector. Contours of SNR as function of redshift z and total binary mass M for the LISA detector are shown in Figure 8.

Full numerical waveforms, and the longer hybrid waveforms generated from them, can also be used to improve existing data-analysis techniques and template sets. Since previously developed gravitational wave data analysis algorithms were not based on knowledge of the merger waveforms, an obvious first step is to test how successfully these techniques detect the merger signals predicted by numerical simulations. In 2009, the NINJA project (82) used direct injection of a broad range of short and long numerical merger waveforms into mock LIGO and Virgo data streams for this purpose. The result was the most realistic testing ground to date for disparate data-analysis methods, including full and partial waveform template matching, as well as unmodeled burst searches. Further studies of detection algorithms with numerical relativity waveforms are continuing.

4.1.2 MEASURING BLACK-HOLE BINARY PARAMETERS The SNR is only a crude guide to the specific detector response to gravitational waveforms, however. The merger portion of the waveform, though short in duration, may contain important new information not present in the inspiral. As a simple example, we expect the time of merger itself to be well localized with the full waveform, whereas it is not well-defined in the inspiral-only signal.

More generally, the different (ℓ, m) modes of a binary's full inspiral-merger-ringdown waveform scale differently with the time to merger. Modes that were

not significant during inspiral suddenly become more prominent in the merger, and the detailed information they carry becomes available to the observer (38,39)

After detection of gravitational waves from distant sources, we are most interested in identifying the physical parameters of the sources. Each of the seven intrinsic parameters of a black-hole binary (mass ratio and spin vectors) will, in general, be imprinted on the gravitational-wave signal, along with some extrinsic parameters such as sky position and distance to the source. For sufficiently strong SNRs, expected for massive binary mergers seen by LISA, we can expect to be able to extract some of these parameters at high precision. While these parameters can be partially disentangled using inspiral-only template information, it has recently been found that the full merger waveform can help break parameter degeneracies and hence drive down uncertainties in several important physical parameters. Good localization of the source on the sky is especially important for the development of multi-messenger astronomy. The recent parameter estimation studies of non-spinning mergers that include the merger waveforms indicate that LISA will be able to locate sky positions within a few arcminutes for binaries with $\sim 10^6 M_\odot$ at cosmological distances (redshift $z = 1$) (83).

4.2 Consequences of Merger Recoil

As previously discussed, asymmetries in a black-hole binary system due to unequal masses and/or spins result in the anisotropic emission of gravitational radiation, ultimately imparting a recoil to the merged remnant black hole. Numerically it has been found that, for certain configurations of black hole spins, the recoil velocity can exceed the escape velocity of many galaxies. Since it is important to determine the theoretical probability that a massive black hole might be

ejected from its host galaxy, there have been some preliminary calculations based on simple distributions of spins and mass ratios, and analytic fits of numerical results giving the dependence of the recoil on mass and spin (84,69). Although a consensus on the exact probability of galactic ejection has yet to be achieved, there is general agreement that it is non-negligible.

Such rogue black holes may have already been observed in the form of two rapidly moving quasars (85). It has been speculated that these particular quasars originated from the mergers of massive black holes during the coalescence of their host galaxies. However a previous study of quasar data found no indications of such recoil events, suggesting that they are rare (86).

The effect of recoil may also be observed less directly in its effect on the growth rates of black holes. Those ejected into the sparse intergalactic medium are less likely to encounter and merge with other black holes (87). Even the growth of recoiled black holes remaining within their host galaxies may be affected, as the motion of the black hole can modify the rate at which it accretes matter (88).

4.3 Mass and Spin Evolution

The expected distribution of masses and spins of astrophysical black holes is another topic of considerable interest in astrophysics. In our current understanding, black holes grow from smaller “seeds” early in the history of the universe through a combination of mergers and the accretion of gas (89). In general, most of the mass growth is believed to come from accretion, with mergers providing a modest increase.

However, the gravitational radiation emitted during black hole coalescence carries away energy, reducing the overall system mass by roughly several percent.

The bulk of this loss happens quickly, in the final plunge and merger stage of the coalescence. With this rapid mass loss, nearby matter in an accretion disk around the remnant black hole might react to the accompanying sudden change in gravitational potential and produce a visible change in its electromagnetic profile – a possible electromagnetic counterpart to the burst of gravitational radiation (90,91).

For the final spin the situation is considerably more interesting, and may answer questions about double-jet “X-shaped” radio sources (92). We have seen in Sec. 3.2 that the final spin from black holes merging in vacuum depends on the magnitudes of the initial spins and their orientations relative to the orbital axis. The RIT group (53) has recently used their extended mass and spin formulas in a spin-evolution study, obtaining asymptotic spin distributions for BH merger remnants assuming no accretion. However, interaction of the merging holes with surrounding gas may serve to align the binary spins before merger, changing the picture somewhat (93). In general, the effects of binary merger and accretion have to be studied together for a coherent picture to emerge (94).

5 Outlook

5.1 Complete Analytic Waveform Models

Gravitational wave observatories may be sensitive to hundreds or thousands of wave cycles. Analysis of the observed data requires comparisons with model signals representing the full variety of possible mergers. Computing so many orbits of pre-merger evolution using numerical relativity would be computationally very expensive.

The PN approximation provides accurate representations of the dynamics and

waveforms for the long-lasting inspiral portion of the coalescence during which the black holes remain fairly well-separated and their velocities remain relatively low. The most valuable waveform models for gravitational wave data analysis must combine the efficiency of the PN approach, while accurately representing the final merger portion of the which is only understood by numerical simulations. This requires a means of analytically encoding the merger signals.

Several approaches are currently being explored for constructing these complete signal models. Some are based on the analytic “effective-one-body” model of binary coalescence (95,96,97). Figure 9 shows a comparison between an effective-one-body waveform for the merger of a nonspinning black hole binary with mass ratio $q = 4$ with a numerically simulated waveform (96). For specific cases, such models have been tuned to high accuracy to agree to agree with numerical results (98). Another approach, which models the phenomenological shape of hybrid waveforms in frequency space (99), has been extended for the dominant waveform modes from spinning, but non-precessing, mergers (100). Further development of these models, and the production of a family of simulated waveform spanning the parameter space, is a current focus of broad-based research collaborations.

5.2 Improved Numerical Methods

5.2.1 INITIAL DATA The initial data models currently used to begin numerical simulations do not perfectly represent the intended astrophysical systems. Research continues to improve these models. For example, although some astrophysical black holes are expected to have near-extremal spins, common initial data cannot represent holes with $(a/M)_i \gtrsim 0.93$ (101, 102); novel methods are being developed to go beyond this limit (101). Also, current initial data mod-

els generally do not contain the physically appropriate radiation content for an inspiraling binary (32, 103), but rather harbor spurious radiation that is not astrophysical (104). Efforts are underway to include initial radiation content more consistent with PN predictions (105). In addition, in the case of moving punctures, the initial coordinates typically undergo a rapid transition at the start of the evolution as the black holes relax into a more stable solution. While the resulting transient pulse of “gauge radiation” does not alter the physics, it does contain fairly high frequencies that can be challenging to resolve and it has motivated construction of analytic initial coordinates that are closer to the numerically evolved coordinates (106).

5.2.2 EVOLUTION More efficient and accurate methods of numerical evolution would make simulations of many binary orbits, particularly with large mass ratios, more computationally practical. For representing spatial derivatives on a computational grid, the highest accuracy of finite differencing stencil yet achieved in the context of numerical relativity is 8th order in the grid spacing (although the accuracy of interpolation between refinement boundaries is not yet commensurate) (107). Spectral methods are generally more accurate but less robust than finite differencing, requiring fine tuning for generic black hole binaries (108); they are also unlikely to handle shocks in accreting matter (see Section 5.3). Alternatives to both finite differencing and spectral methods, such as finite element methods, are also being investigated (109). Meanwhile more efficient time-integration techniques allowing larger step sizes are being explored (110).

5.2.3 WAVE EXTRACTION Because the physical domain of a typical simulation is finite, gravitational radiation is usually extracted on a sphere of finite

radius rather than at infinity. If multiple extraction surfaces are employed in a region of sufficiently high spatial resolution, then the radiation can be extrapolated to spatial infinity. A more accurate method known as “Cauchy-characteristic extrapolation” extracts the gravitational wave data at a finite radius and then evolves it along null geodesics to future null infinity; this method is currently under development (111).

5.3 Including Gas and Magnetic Fields

In addition to being gravitationally “loud”, black hole mergers may also be electromagnetically visible. Massive black holes at the centers of galaxies are typically surrounded by gaseous accretion disks and magnetic fields. When the black holes merge, the dynamics of the gas and magnetic fields may produce electromagnetic signals, counterparts to the emitted gravitational radiation. For example, the inspiral may “twist” the fields, resulting in characteristic electromagnetic radiation (112, 113) as well as heating of a surrounding accretion disk (114). In addition, the violent merger dynamics may induce shock waves in accreting matter, in turn generating electromagnetic radiation. The recoil of the merged remnant, in particular, may have such an effect on the accretion disk (115, 116, 117, 90, 118, 119, 91, 120).

5.3.1 MULTIMESSENGER ASTRONOMY Detection of electromagnetic counterparts of gravitational waves would be of great scientific value. Current models of the complex merger physics (e.g. (121)) could be directly tested. Einstein-Maxwell theory, the coupling of gravitational and electromagnetic fields on macroscopic scales, could be verified. In particular, equality of the speed of gravity with the speed of light could be confirmed (118, 112). Astronomy would

also benefit enormously, as the location and characteristics of gravitational wave sources could be corroborated. In addition, electromagnetically visible mergers could serve as “standard candles”, beacons by which to measure the accelerating expansion of the universe, while simultaneously playing the role of “standard sirens” emitting gravitational radiation. Cross-correlating these signals could result in measurement of the cosmological “dark energy” to unprecedented accuracy (122, 116, 123, 118, 124).

5.3.2 MODELING MATTER There has been some preliminary work on the dynamic effects of the spacetime of a coalescing binary on surrounding matter. Modeling the accretion disk as geodesic particles, large collision energies were found as the binary merged (125). And hydrodynamically simulating a gas cloud around around the binary, luminosity due to shocks has been calculated (126). The generation of electromagnetic radiation by more direct means has also been simulated, via the twisting of a magnetic field anchored in the accretion disk, as it is frame-dragged by the binary (127, 113, 112). Future efforts will employ magnetohydrodynamic methods, where challenges include adequately resolving shocks and turbulence in a dynamic spacetime, and accurately representing the divergence-free magnetic field on an adaptively refined grid.

6 Conclusion

We hope to have conveyed some of the excitement of recent progress in understanding black-hole binary physics, and the applications of this knowledge in astrophysics. These advances are the result of sustained efforts by a broad scientific community over many years. In a brief review, it is impossible to adequately represent all of the excellent work that has contributed to the current state of

knowledge. We have only been able to provide a few of the highlights as seen through the lens of our particular perspective.

We encourage interested readers to pursue the subject further. Other resources are available on topics including: numerical relativity techniques (128,3), the breakthroughs in black hole merger simulations (129), black hole simulations for gravitational wave data analysis (130), and gravitational wave science generally (131,81).

Acknowledgments

We acknowledge support from NASA grants 06-BEFS06-19 and 08-ATFP08-0126. BJK was supported in part by an appointment to the NASA Postdoctoral Program at the Goddard Space Flight Center, administered by Oak Ridge Associated Universities through a contract with NASA.

LITERATURE CITED

1. Arnowitt R, Deser S, Misner CW, The dynamics of general relativity in *Gravitation: An Introduction to Current Research*, , pp. 227–265, Wiley, New York, 1962, arXiv:gr-qc/0405109.
2. Misner CW, Thorne KS, Wheeler JA, *Gravitation* (W. H. Freeman, San Francisco, 1973).
3. Alcubierre M, *Introduction to 3+1 Numerical Relativity* (Oxford University Press, Oxford, U.K., 2008).
4. Smarr LL, York JW, *Phys. Rev. D* 17:2529 (1978).
5. Alcubierre M, Brügmann B, Diener P, Koppitz M, Pollney D, et al., *Phys. Rev. D* 67:084023 (2003), arXiv:gr-qc/0206072.

6. Brügmann B, *Int. J. Mod. Phys. D* 8:85 (1999), arXiv:gr-qc/9708035.
7. Alcubierre M, Bengert W, Brügmann B, Lanfermann G, Nerges L, et al., *Phys. Rev. Lett.* 87:271103 (2001), arXiv:gr-qc/0012079.
8. Baker JG, Campanelli M, *Phys. Rev. D* 62:127501 (2000), arXiv:gr-qc/0003031. Baker JG, Campanelli M, Lousto CO, *Phys. Rev. D* 65:044001 (2002), arXiv:gr-qc/0104063.
9. Baker JG, Campanelli M, Lousto CO, Takahashi R, *Phys. Rev. D* 65:124012 (2002), arXiv:astro-ph/0202469.
10. Baker JG, Campanelli M, Lousto CO, Takahashi R, *Phys. Rev. D* 69:027505 (2004), arXiv:astro-ph/0305287.
11. Campanelli M, *Class. Quantum Grav.* 22:S387 (2005), arXiv:astro-ph/0411744.
12. Shibata M, Nakamura T, *Phys. Rev. D* 52:5428 (1995). Baumgarte TW, Shapiro SL, *Phys. Rev. D* 59:024007 (1998), arXiv:gr-qc/9810065.
13. York JW, Kinematics and dynamics of general relativity in *Sources of Gravitational Radiation*, , pp. 83–126, Cambridge University Press, Cambridge, England, 1979.
14. Nagy G, Ortiz OE, Reula OA, *Phys. Rev. D* 70:044012 (2004), arXiv:gr-qc/0402123. Reula OA, *Journal of Hyperbolic Differential Equations* 1:251 (2004), arXiv:gr-qc/0403007.
15. Anninos P, Camarda K, Massó J, Seidel E, Suen WM, Towns J, *Phys. Rev. D* 52:2059 (1995), arXiv:gr-qc/9503025.
16. Alcubierre M, Brügmann B, Pollney D, Seidel E, Takahashi R, *Phys. Rev. D* 64:61501 (R) (2001), arXiv:gr-qc/0104020. Alcubierre M, *Class. Quantum Grav.* 20:607 (2003), arXiv:gr-qc/0210050.

17. Thornburg J, *Class. Quantum Grav.* 4:1119 (1987).
18. Brandt SR, Brügmann B, *Phys. Rev. Lett.* 78:3606 (1997),
arXiv:gr-qc/9703066.
19. Shoemaker DM, Smith KL, Sperhake U, Laguna P, Schnetter E, Fiske DR,
Class. Quantum Grav. 20:3729 (2003), arXiv:gr-qc/0301111.
20. Alcubierre M, Brügmann B, *Phys. Rev. D* 63:104006 (2001),
arXiv:gr-qc/0008067.
21. Alcubierre M, Brügmann B, Diener P, Guzmán FS, Hawke I, et al., *Phys.*
Rev. D 72:044004 (2005), arXiv:gr-qc/0411149.
22. Brügmann B, Tichy W, Jansen N, *Phys. Rev. Lett.* 92:211101 (2004),
arXiv:gr-qc/0312112.
23. Pretorius F, *Phys. Rev. Lett.* 95:121101 (2005), arXiv:gr-qc/0507014.
24. Pretorius F, *Class. Quantum Grav.* 23:S529 (2006), arXiv:gr-qc/0602115.
25. Pretorius F, *Class. Quantum Grav.* 22:425 (2005), arXiv:gr-qc/0407110.
26. Gundlach C, Martín-García JM, Calabrese G, Hinder I, *Class. Quantum*
Grav. 22:3767 (2005), arXiv:gr-qc/0504114.
27. Campanelli M, Lousto CO, Marronetti P, Zlochower Y, *Phys. Rev. Lett.*
96:111101 (2006), arXiv:gr-qc/0511048.
28. Baker JG, Centrella JM, Choi DI, Koppitz M, van Meter JR, *Phys. Rev.*
Lett. 96:111102 (2006), arXiv:gr-qc/0511103.
29. van Meter JR, Baker JG, Koppitz M, Choi DI, *Phys. Rev. D* 73:124011
(2006), arXiv:gr-qc/0605030.
30. Peters PC, Mathews J, *Phys. Rev.* 131:435 (1963). Peters PC, *Phys. Rev.*
136:B1224 (1964).
31. Lousto CO, Price RH, *Phys. Rev. D* 57:1073 (1998), arXiv:gr-qc/9708022.

- 32. Damour T, Jaranowski P, Schäfer G, *Phys. Rev. D* 62:084011 (2000),
arXiv:gr-qc/0005034.
- 33. Pfeiffer HP, Cook GB, Teukolsky SA, *Phys. Rev. D* 66:024047 (2002),
arXiv:gr-qc/0203085.
- 34. Baker JG, Centrella JM, Choi DI, Koppitz M, van Meter JR, *Phys. Rev. D*
73:104002 (2006), arXiv:gr-qc/0602026.
- 35. Hinder I, Vaishnav B, Herrmann F, Shoemaker DM, Laguna P, *Phys. Rev.*
D 77:081502(R) (2008), arXiv:0710.5167 [gr-qc].
- 36. Bode T, Shoemaker DM, Herrmann F, Hinder I, *Phys. Rev. D* 77:044027
(2008), arXiv:0711.0669 [gr-qc].
- 37. Gonzalez JA, Sperhake U, Brügmann B, *Phys. Rev. D* 79:124006 (2009),
arXiv:0811.3952 [gr-qc].
- 38. Berti E, Cardoso V, Gonzalez JA, Sperhake U, Hannam MD, et al., *Phys.*
Rev. D 76:064034 (2007), arXiv:gr-qc/0703053.
- 39. Baker JG, Boggs WD, Centrella JM, Kelly BJ, McWilliams ST, van Meter
JR, *Phys. Rev. D* 78:044046 (2008), arXiv:0805.1428 [gr-qc].
- 40. Apostolatos TA, Cutler C, Sussman GJ, Thorne KS, *Phys. Rev. D* 49:6274
(1994). Kidder LE, *Phys. Rev. D* 52:821 (1995), arXiv:gr-qc/9506022.
- 41. Campanelli M, Lousto CO, Zlochower Y, *Phys. Rev. D* 74:041501(R) (2006),
arXiv:gr-qc/0604012.
- 42. Campanelli M, Lousto CO, Zlochower Y, Krishnan B, Merritt D, *Phys. Rev.*
D 75:064030 (2007), arXiv:gr-qc/0612076.
- 43. Campanelli M, Lousto CO, Zlochower Y, Merritt D, *Astrophys. J.* 659:L5
(2007), arXiv:gr-qc/0701164.
- 44. Campanelli M, Lousto CO, Nakano H, Zlochower Y, *Phys. Rev. D* 79:084010

- (2009), arXiv:0808.0713 [gr-qc].
45. Berti E, Cardoso V, Gonzalez JA, Sperhake U, Brügmann B, *Class. Quantum Grav.* 25:114035 (2008), arXiv:0711.1097 [gr-qc].
 46. Scheel MA, Boyle M, Chu T, Kidder LE, Matthews KD, Pfeiffer HP, *Phys. Rev. D* 79:024003 (2009), arXiv:0810.1767 [gr-qc].
 47. Campanelli M, Lousto CO, Zlochower Y, *Phys. Rev. D* 74:084023 (2006), arXiv:astro-ph/0608275.
 48. Pollney D, Reisswig C, Rezzolla L, Szilágyi B, Ansorg M, et al., *Phys. Rev. D* 76:124002 (2007), arXiv:0707.2559 [gr-qc].
 49. Buonanno A, Kidder LE, Lehner L, *Phys. Rev. D* 77:026004 (2008), arXiv:0709.3839 [astro-ph].
 50. Tichy W, Marronetti P, *Phys. Rev. D* 76:061502(R) (2007), arXiv:gr-qc/0703075.
 51. Dain S, Lousto CO, Zlochower Y, *Phys. Rev. D* 78:024039 (2008), arXiv:0803.0351 [gr-qc].
 52. Kesden M, *Phys. Rev. D* 78:084030 (2008), arXiv:0807.3043 [gr-qc]. Rezzolla L, Dorband EN, Reisswig C, Diener P, Pollney D, et al., *Astrophys. J.* 679:1422 (2008), arXiv:0708.3999 [gr-qc]. Rezzolla L, Diener P, Dorband EN, Pollney D, Reisswig C, et al., *Astrophys. J.* 674:L29 (2008), arXiv:0710.3345 [gr-qc]. Rezzolla L, Barausse E, Dorband EN, Pollney D, Reisswig C, et al., *Phys. Rev. D* 78:044002 (2008), arXiv:0712.3541 [gr-qc]. Tichy W, Marronetti P, *Phys. Rev. D* 78:081501(R) (2008), arXiv:0807.2985 [gr-qc].
 53. Lousto CO, Campanelli M, Zlochower Y, *Class. Quantum Grav.* 27:114006 (2010), arXiv:0904.3541 [gr-qc].
 54. Rezzolla L, *Class. Quantum Grav.* 26:094023 (2009), arXiv:0812.2325 [gr-

- qc], Proceedings of 7th LISA Symposium, Barcelona June 2008.
55. Healy J, Laguna P, Matzner RA, Shoemaker DM, *Phys. Rev. D* 81:081501 (2010), arXiv:0905.3914 [gr-qc].
56. Sperhake U, Cardoso V, Pretorius F, Berti E, Hinderer T, Yunes N, *Phys. Rev. Lett.* 103:131102 (2009), arXiv:0907.1252 [gr-qc].
57. Fitchett MJ, *Mon. Not. R. Astron. Soc.* 203:1049 (1983).
58. Favata M, Hughes SA, Holz DE, *Astrophys. J.* 607:L5 (2004), arXiv:astro-ph/0402056. Blanchet L, Qusailah MSS, Will CMW, *Astrophys. J.* 635:508 (2005), arXiv:astro-ph/0507692. Damour T, Gopakumar A, *Phys. Rev. D* 73:124006 (2006), arXiv:gr-qc/0602117. Wiseman AG, *Phys. Rev. D* 46:1517 (1992).
59. Herrmann F, Shoemaker DM, Laguna P, *Class. Quantum Grav.* 24:S33 (2007), arXiv:gr-qc/0601026.
60. Baker JG, Centrella JM, Choi DI, Koppitz M, van Meter JR, Miller MC, *Astrophys. J.* 653:L93 (2006), arXiv:astro-ph/0603204.
61. Gonzalez JA, Sperhake U, Brüggmann B, Hannam MD, Husa S, *Phys. Rev. Lett.* 98:091101 (2007), arXiv:gr-qc/0610154.
62. Herrmann F, Hinder I, Shoemaker DM, Laguna P, Matzner RA, *Astrophys. J.* 661:430 (2007), arXiv:gr-qc/0701143. Koppitz M, Pollney D, Reisswig C, Rezzolla L, Thornburg J, et al., *Phys. Rev. Lett.* 99:041102 (2007), arXiv:gr-qc/0701163.
63. Gonzalez JA, Hannam MD, Sperhake U, Brüggmann B, Husa S, *Phys. Rev. Lett.* 98:231101 (2007), arXiv:gr-qc/0702052.
64. Brüggmann B, Gonzalez JA, Hannam MD, Husa S, Sperhake U, *Phys. Rev. D* 77:124047 (2008), arXiv:0707.0135 [gr-qc].

65. Schnittman JD, Buonanno A, van Meter JR, Baker JG, Boggs WD, et al., *Phys. Rev. D* 77:044031 (2008), arXiv:0707.0301 [gr-qc].
66. Baker JG, Boggs WD, Centrella JM, Kelly BJ, McWilliams ST, et al., *Astrophys. J.* 668:1140 (2007), arXiv:astro-ph/0702390.
67. Campanelli M, Lousto CO, Zlochower Y, Merritt D, *Phys. Rev. Lett.* 98:231102 (2007), arXiv:gr-qc/0702133.
68. Lousto CO, Zlochower Y, *Phys. Rev. D* 77:044028 (2007), arXiv:0708.4048.
69. Baker JG, Boggs WD, Centrella JM, Kelly BJ, McWilliams ST, et al., *Astrophys. J.* 682:L29 (2008), arXiv:0802.0416 [astro-ph].
70. Lousto CO, Zlochower Y, *Phys. Rev. D* 79:064018 (2009), arXiv:0805.0159 [gr-qc].
71. Boyle M, Brown DA, Kidder LE, Mroué AH, Pfeiffer HP, et al., *Phys. Rev. D* 76:124038 (2007), arXiv:0710.0158 [gr-qc].
72. Husa S, Hannam MD, Gonzalez JA, Sperhake U, Brügmann B, *Phys. Rev. D* 77:044037 (2008), arXiv:0706.0904 [gr-qc].
73. Baker JG, van Meter JR, McWilliams ST, Centrella JM, Kelly BJ, *Phys. Rev. Lett.* 99:181101 (2007), arXiv:gr-qc/0612024.
74. Baker JG, McWilliams ST, van Meter JR, Centrella JM, Choi DI, et al., *Phys. Rev. D* 75:124024 (2007), arXiv:gr-qc/0612117.
75. Hannam MD, Husa S, Sperhake U, Brügmann B, Gonzalez JA, *Phys. Rev. D* 77:044020 (2007), arXiv:0706.1305 [gr-qc].
76. Lindblom L, Scheel MA, Kidder LE, Owen R, Rinne O, *Class. Quantum Grav.* 23:S447 (2006), arXiv:gr-qc/0512093. Scheel MA, Pfeiffer HP, Lindblom L, Kidder LE, Rinne O, Teukolsky SA, *Phys. Rev. D* 74:104006 (2006), arXiv:gr-qc/0607056.

- 77. Chu T, Pfeiffer HP, Scheel MA, *Phys. Rev. D* 80:124051 (2009), arXiv:0909.1313 [gr-qc].
- 78. Hannam MD, Husa S, Baker JG, Boyle M, Brüggmann B, et al., *Phys. Rev. D* 79:084025 (2009), arXiv:0901.2437 [gr-qc].
- 79. Hannam MD, Husa S, Brüggmann B, Gopakumar A, *Phys. Rev. D* 78:104007 (2008), arXiv:0712.3787 [gr-qc].
- 80. Pan Y, Buonanno A, Buchman LT, Chu T, Kidder LE, et al., *Phys. Rev. D* 81:084041 (2010), arXiv:0912.3466 [gr-qc].
- 81. Camp JB, Cornish NJ, *Annu. Rev. Nucl. Part. Sci.* 54:525 (2004).
- 82. Aylott B, et al., *Class. Quantum Grav.* 26:165008 (2009), arXiv:0901.4399 [gr-qc].
- 83. McWilliams ST, Thorpe JJ, Baker JG, Kelly BJ, *Phys. Rev. D* 81:064014 (2010), arXiv:0911.1078 [gr-qc].
- 84. Schnittman JD, Buonanno A, *Astrophys. J.* 662:L63 (2007), arXiv:astro-ph/0702641.
- 85. Shields GA, Rosario DJ, Smith KL, Bonning EW, Salviander S, et al., *Astrophys. J.* 707:936 (2009), arXiv:0907.3470 [astro-ph.CO]. Komossa S, Zhou H, Lu H, *Astrophys. J.* 678:L81 (2008), arXiv:0804.4584 [astro-ph].
- 86. Bonning EW, Shields GA, Salivander S, *Astrophys. J.* 666:L13 (2007), arXiv:0705.4263 [astro-ph].
- 87. Sesana A, Volonteri M, Haardt F, *Mon. Not. R. Astron. Soc.* 377:1711 (2007), arXiv:astro-ph/0701556. Volonteri M, *Astrophys. J.* 663:L5 (2007), arXiv:astro-ph/0703180.
- 88. Blecha L, Loeb A, *Mon. Not. R. Astron. Soc.* 390:1311 (2008), arXiv:0805.1420 [gr-qc].

89. Sesana A, Haardt F, Madau P, Volonteri M, *Astrophys. J.* 611:623 (2004),
arXiv:astro-ph/0401543.
90. Bode N, Phinney S, *APS Meeting Abstracts* :1010 (2007).
91. O’Neill SM, Miller MC, Bogdanovic T, Reynolds CS, Schnittman J, *Astrophys. J.* 700:859 (2009), arXiv:0812.4874 [astro-ph].
92. Merritt D, Ekers RD, *Science* 297:1310 (2002), arXiv:astro-ph/0208001.
Barausse E, Rezzolla L, *Astrophys. J.* 704:L40 (2009), arXiv:0904.2577 [gr-qc].
93. Bogdanovic T, Reynolds CS, Miller MC, *Astrophys. J.* 661:L147 (2007),
arXiv:astro-ph/0703054.
94. Berti E, Volonteri M, *Astrophys. J.* 684:822 (2008), arXiv:0802.0025 [astro-ph].
95. Pan Y, Buonanno A, Baker JG, Centrella JM, Kelly BJ, et al., *Phys. Rev. D* 77:024014 (2008), arXiv:0704.1964 [gr-qc].
96. Buonanno A, Pan Y, Baker JG, Centrella JM, Kelly BJ, et al., *Phys. Rev. D* 76:104049 (2007), arXiv:0706.3732 [gr-qc].
97. Damour T, Nagar A, Hannam MD, Husa S, Brügmann B, *Phys. Rev. D* 78:044039 (2008), arXiv:0803.3162 [gr-qc].
98. Damour T, Nagar A, *Phys. Rev. D* 79:081503(R) (2009), arXiv:0902.0136 [gr-qc].
Buonanno A, Pan Y, Pfeiffer HP, Scheel MA, Buchman LT, Kidder LE, *Phys. Rev. D* 79:124028 (2009), arXiv:0902.0790 [gr-qc].
99. Ajith P, Babak S, Chen Y, Hewitson M, Krishnan B, et al., *Phys. Rev. D* 77:104017 (2008), Erratum: *ibid.* **79**, 129901(E) (2009), arXiv:0710.2335 [gr-qc].
100. Ajith P, Hannam MD, Husa S, Chen Y, Brügmann B, et al., arXiv:0909.2867

- [gr-qc], 2009.
101. Lovelace G, Owen R, Pfeiffer HP, , Chu T, *Phys. Rev. D* 78:084017 (2008),
arXiv:0805.4192 [gr-qc].
 102. Dain S, Lousto CO, Takahashi R, *Phys. Rev. D* 65:104038 (2002),
arXiv:gr-qc/0201062.
 103. Pfeiffer HP, *Initial data for black hole evolutions*, PhD thesis, Cornell
University, 2005, arXiv:gr-qc/0510016.
 104. Hannam MD, Husa S, Brüggmann B, Gonzalez JA, Sperhake U, *Class.*
Quantum Grav. 24:S15 (2007), arXiv:gr-qc/0612001.
 105. Kelly BJ, Tichy W, Campanelli M, Whiting BF, *Phys. Rev. D* 76:024008
(2007), arXiv:0704.0628 [gr-qc].
 106. Hannam MD, Husa S, Ó Murchadha N, *Phys. Rev. D* 80:124007 (2009),
arXiv:0908.1063 [gr-qc].
 107. Lousto CO, Zlochower Y, *Phys. Rev. D* 77:024034 (2008), arXiv:0711.1165
[gr-qc]. Pollney D, Reisswig C, Schnetter E, Dorband EN, Diener P,
arXiv:0910.3803 [gr-qc], 2009.
 108. Szilágyi B, Lindblom L, Scheel MA, arXiv:0909.3557 [gr-qc], 2009.
 109. Zumbusch G, *Class. Quantum Grav.* 26:175011 (2009), arXiv:0901.0851
[gr-qc].
 110. Lau SR, Pfeiffer HP, Hesthaven JS, *Commun. Comput. Phys.* 6:1063 (2009),
arXiv:0808.2597 [gr-qc].
 111. Reisswig C, Bishop NT, Pollney D, Szilágyi B, *Class. Quantum Grav.*
27:075014 (2010), arXiv:0912.1285 [gr-qc]. Babiuc MC, Bishop NT, Szilagy
B, Winicour J, *Phys. Rev. D* 79:084011 (2009), arXiv:0808.0861 [gr-qc].
 112. Palenzuela C, Anderson M, Lehner L, Liebling SL, Neilsen D, *Phys. Rev.*

- Lett.* 103:081101 (2009), arXiv:0905.1121 [astro-ph.HE].
113. Palenzuela C, Lehner L, Yoshida S, *Phys. Rev. D* 81:084007 (2010), arXiv:0911.3889 [gr-qc].
114. Reynolds CS, Garofalo D, Begelman MC, *Astrophys. J.* 651:1023 (2006), arXiv:astro-ph/0607381.
115. Armitage PJ, Natarajan P, *Astrophys. J.* 567:L9 (2002), arXiv:astro-ph/0201318. Milosavljevic M, Phinney ES, *Astrophys. J.* 622:L93 (2005), arXiv:astro-ph/0410343. Dotti M, Salvaterra R, Sesana A, Colpi M, Haardt F, *Mon. Not. R. Astron. Soc.* 372:869 (2006), arXiv:astro-ph/0605624.
116. Kocsis B, Frei Z, Haiman Z, Menou K, *Astrophys. J.* 637:27 (2006), arXiv:astro-ph/0505394.
117. Phinney ES, Binary black hole evolutions with moving punctures: methods and numerical codes, 2007, Bulletin of the 2007 APS April Meeting, abstract T7.00002.
118. Kocsis B, Haiman Z, Menou K, *Astrophys. J.* 684:870 (2008), arXiv:0712.1144.
119. Shields GA, Bonning EW, *Astrophys. J.* 682:758 (2008), arXiv:0802.3873 [astro-ph]. Lippai Z, Frei Z, Haiman Z, *Astrophys. J.* 676:L5 (2008), arXiv:0801.0739 [astro-ph]. Schnittman JD, Krolik JH, *Astrophys. J.* 684:835 (2008), arXiv:0802.3556 [astro-ph]. Kocsis B, Loeb A, *Phys. Rev. Lett.* 101:041101 (2008), arXiv:0803.0003 [astro-ph]. Haiman Z, Kocsis B, Menou K, Lippai Z, Frei Z, *Class. Quantum Grav.* 26:094032 (2009), arXiv:0811.1920 [astro-ph].
120. Haiman Z, Kocsis B, Menou K, *Astrophys. J.* 700:1952 (2009),

- arXiv:0904.1383 [astro-ph.CO]. Chang P, Strubbe LE, Menou K, Quataert E, arXiv:0906.0825 [astro-ph.HE], 2009. Megevand M, et al., *Phys. Rev. D* 80:024012 (2009), arXiv:0905.3390 [astro-ph.HE].
121. Balbus SA, Hawley JF, *Astrophys. J.* 376:214 (1991).
 122. Lang RN, Hughes SA, *Class. Quantum Grav.* 26:094035 (2009), arXiv:0810.5125 [astro-ph]. Kocsis B, Haiman Z, Menou K, Frei Z, *Phys. Rev. D* 76:022003 (2007), arXiv:astro-ph/0701629. Jonsson J, Goobar A, Mortsell E, *Astrophys. J.* 658:52 (2007), arXiv:astro-ph/0611334. Dalal N, Holz DE, Hughes SA, Jain B, *Phys. Rev. D* 74:063006 (2006), arXiv:astro-ph/0601275.
 123. Holz DE, Hughes SA, *Astrophys. J.* 629:15 (2005), arXiv: astro-ph/0504616.
 124. Arun KG, Mishra CK, van den Broeck C, Iyer BR, Sathyaprakash BS, Sinha S, *Class. Quantum Grav.* 26:094021 (2009), arXiv:0810.5727 [gr-qc].
 125. van Meter JR, Wise JH, Miller MC, Reynolds CS, Centrella JM, et al., *Astrophys. J.* 711:L89 (2010), arXiv:0908.0023 [astro-ph.HE].
 126. Bode T, Haas R, Bogdanovic T, Laguna P, Shoemaker DM, *Astrophys. J.* 715:1117 (2010), arXiv:0912.0087 [gr-qc].
 127. Mösta P, Palenzuela C, Rezzolla L, Lehner L, Yoshida S, Pollney D, *Phys. Rev. D* 81:064017 (2010), arXiv:0912.2330 [gr-qc].
 128. Bona C, Palenzuela-Luque C, *Elements of Numerical Relativity* volume 673 of *Lecture Notes in Physics* (Springer, Berlin/Heidelberg, 2005).
 129. Pretorius F, Binary black hole coalescence in *Physics of Relativistic Objects in Compact Binaries: from Birth to Coalescence*, , pp. 305–369, Springer, Heidelberg, Germany, 2009, arXiv:0710.1338 [gr-qc].
 130. Hannam MD, *Class. Quantum Grav.* 26:114001 (2009), arXiv:0901.2931

[gr-qc].

131. Sathyaprakash BS, Schutz BF, *Living Rev. Relativity* 12:2 (2009),
arXiv:0903.0338 [gr-qc], <http://www.livingreviews.org/lrr-2009-2>.

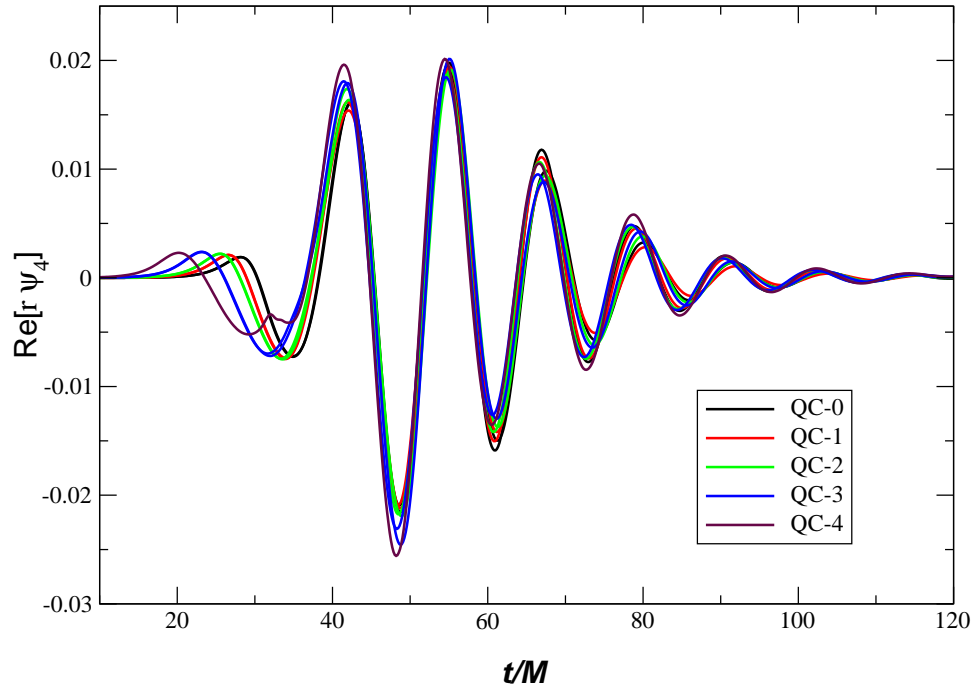


Figure 1: Waveforms from Lazarus models of equal-mass, nonspinning black hole mergers. This figure shows the $\ell = 2, m = 2$ component of $\text{Re}(r\Psi_4)$, corresponding to one of the two polarization states of the emitted gravitational radiation. Curves are plotted for 10 simulations having different initial black hole separations (designated QC-0, etc.) and transition times to perturbative evolution. Reprinted from (9) and copyright 2002 by the American Physical Society (<http://link.aps.org/abstract/PRD/v65/e124012>).

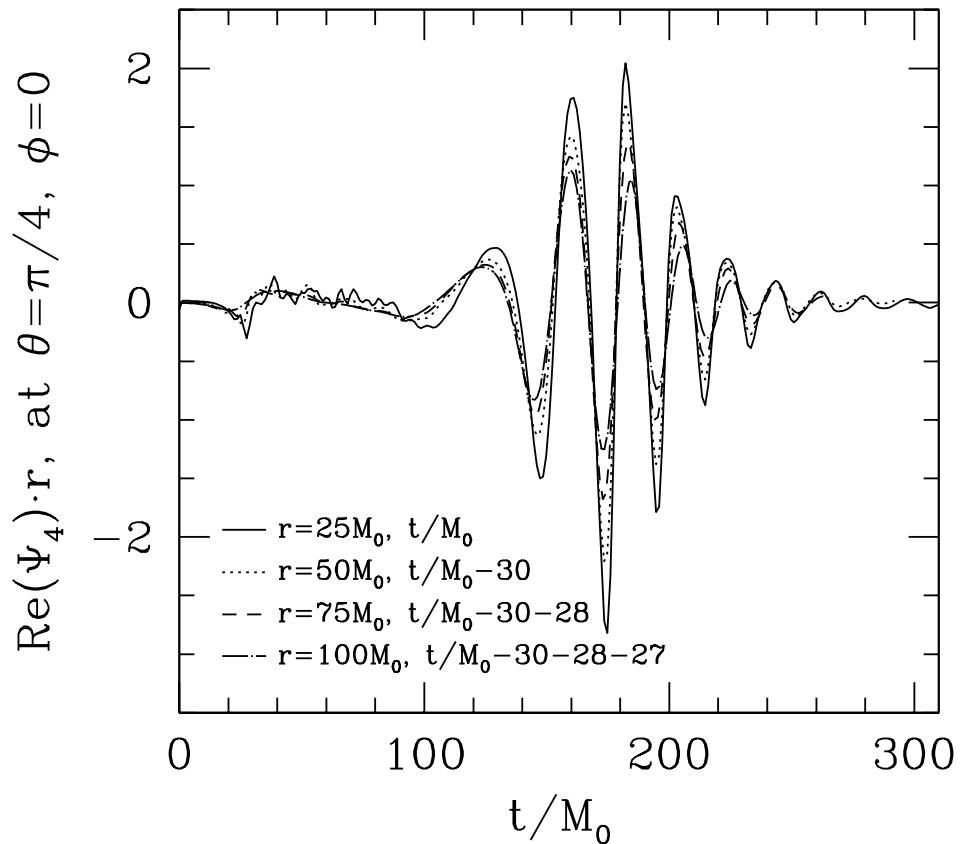


Figure 2: The first gravitational waveform for binary of equal-mass black holes evolving through a single plunge orbit, merger, and ringdown, computed by Pretorius. The waveforms were extracted at four radii from the source, and then shifted in time to overlap for comparison. Reprinted with permission from (23) and copyright 2005 by the American Physical Society (<http://link.aps.org/abstract/PRL/v95/e121101>).

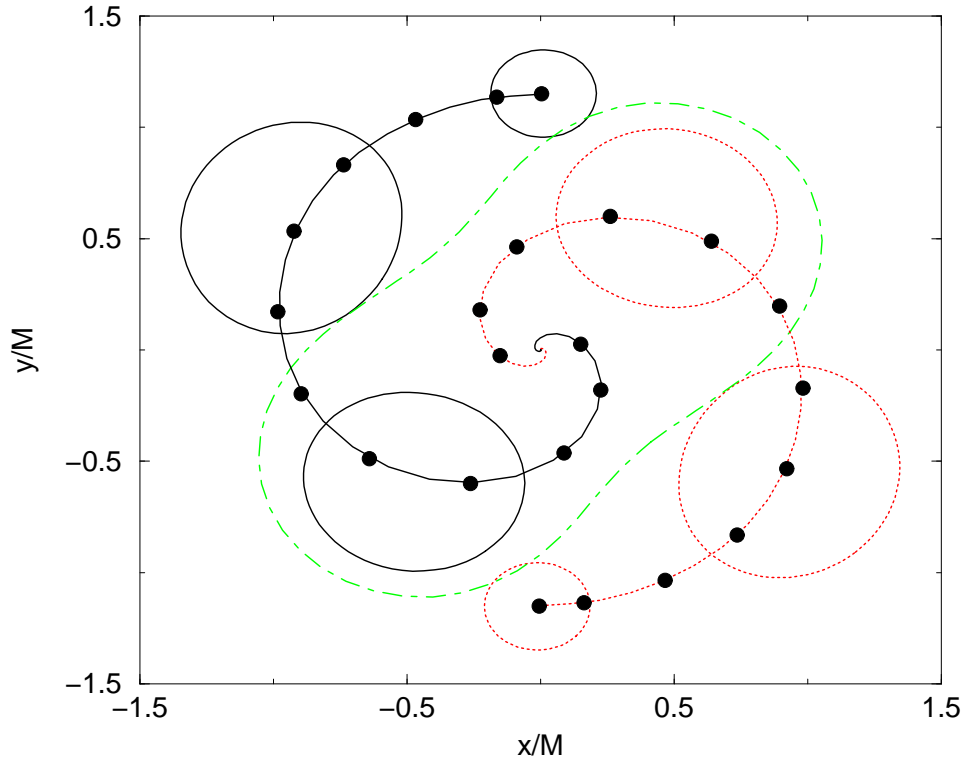


Figure 3: Puncture trajectories from the merger of an equal-mass nonspinning black-hole binary calculated by the UTB group. The apparent horizons of the two pre-merger holes, outlined in solid (black) and red (dashed), expand due to coordinate effects. Also shown is the first detected common horizon, outlined in green (dot-dashed); this designates the point of merger and has a “peanut” shape before it settles down. Reprinted with permission from (27) and copyright 2006 by the American Physical Society (<http://link.aps.org/abstract/PRL/v96/e111101>).

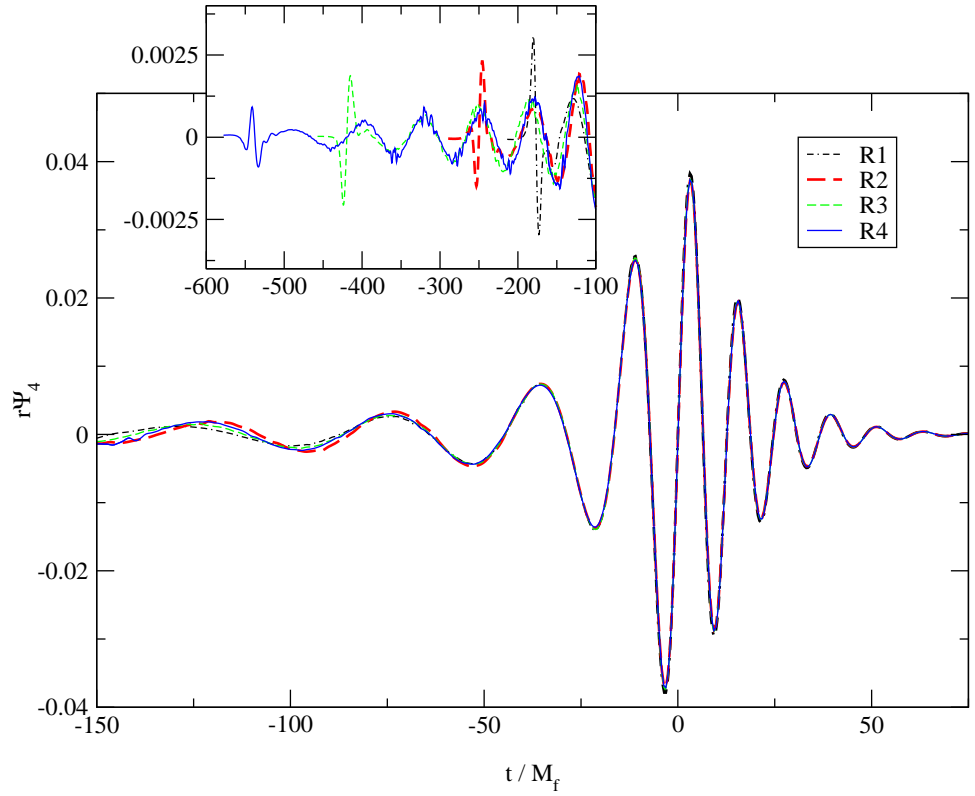


Figure 4: The universal waveform for equal-mass, nonspinning black holes calculated by the GSFC group. The figure shows waveforms from four simulations with increasingly larger initial separations between the black holes. These waveforms were shifted in time so that the peak radiation amplitude occurs at $t = 0$. Reprinted from (34) and copyright 2006 by the American Physical Society (<http://link.aps.org/abstract/PRD/v73/e104002>).

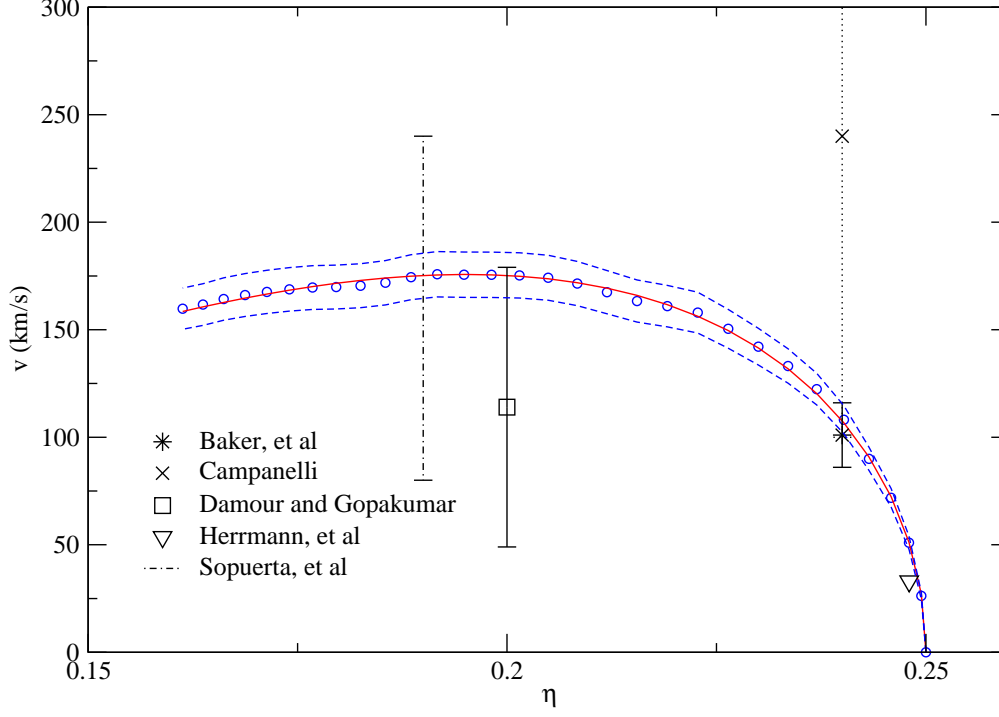


Figure 5: Recoil kicks for nonspinning black-hole mergers for mass ratios $q \in \{1.0, 3.95\}$, or $\eta \in \{0.161, 0.25\}$; here, $\eta = q/(1 + q)^2$. The open circles are the results obtained from numerical relativity simulations by Gonzalez et al. (61), with a functional fit given by the continuous (red) line, and uncertainties of $\sim 6\%$ indicated by the dashed (blue) lines above and below. For comparison, earlier numerical results (discrete symbols with error bars) are also shown. Reprinted with permission from (61) and copyright 2007 by the American Physical Society (<http://link.aps.org/abstract/PRL/v98/e091101>).

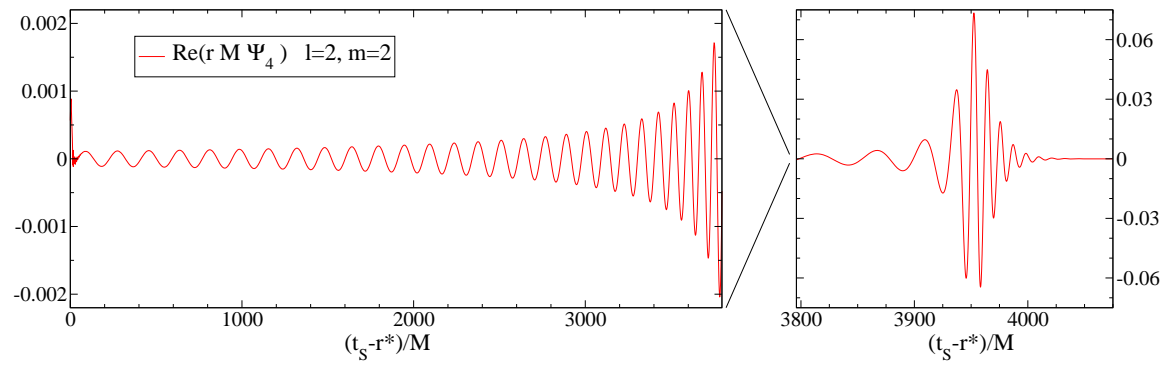


Figure 6: The longest gravitational waveform for an equal-mass, nonspinning black-hole binary merger computed by the Caltech-Cornell group. The left panel shows the early stages of the waveform, during the inspiral. The right panel displays the merger and ringdown portions of the waveform. Reprinted with permission from (46) and copyright 2009 by the American Physical Society (<http://link.aps.org/abstract/PRD/v79/e024003>).

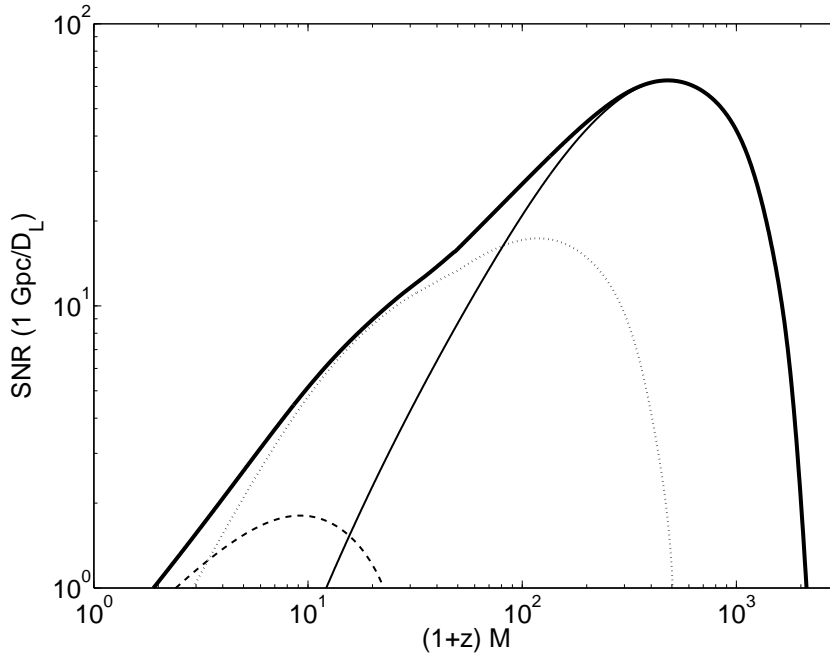


Figure 7: Gain in SNR by including the merger segment of the waveform for an equal-mass, nonspinning binary. The SNR for sources located at luminosity distance $D_L = 1$ Gpc is plotted vs. (redshifted) mass for the Advanced LIGO detector. The dashed line shows the SNR calculated using PN techniques for the early inspiral part of the waveform, $-\infty < t < -1000M$. The dotted line shows the SNR using the late inspiral, $-1000M < t < -50M$, which is the transition region from PN to numerical relativity. The SNR for the strong-field merger and ringdown, $-50M < t < \infty$, was calculated using waveforms from a numerical relativity simulation and is shown using a thin solid line. Finally, the SNR from the entire waveform is given as the thick solid line. Here, $t = 0$ marks the time of maximum gravitational radiation amplitude. Reprinted from (74) and copyright 2007 by the American Physical Society (<http://link.aps.org/abstract/PRD/v75/e124024>).

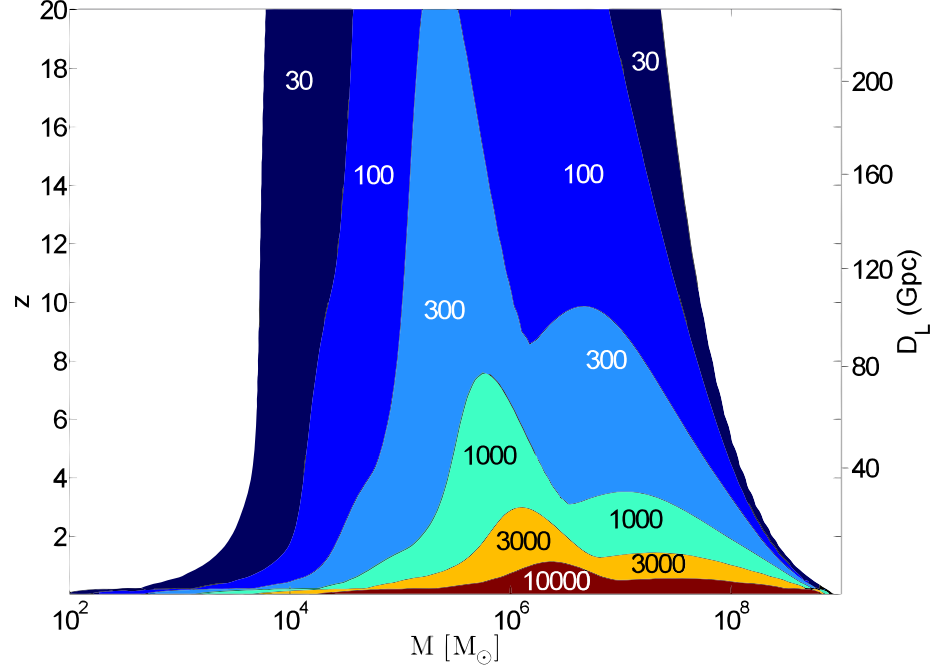


Figure 8: Contours of SNR as a function of redshift z and total binary mass M are shown for the LISA detector. These have been calculated using a hybrid equal-mass nonspinning waveform: using PN for the early inspiral, matching to a numerical relativity waveform in the late inspiral, and continuing with the numerical waveform through the merger and ringdown. Reprinted from (74) and copyright 2007 by the American Physical Society (<http://link.aps.org/abstract/PRD/v75/e124024>).

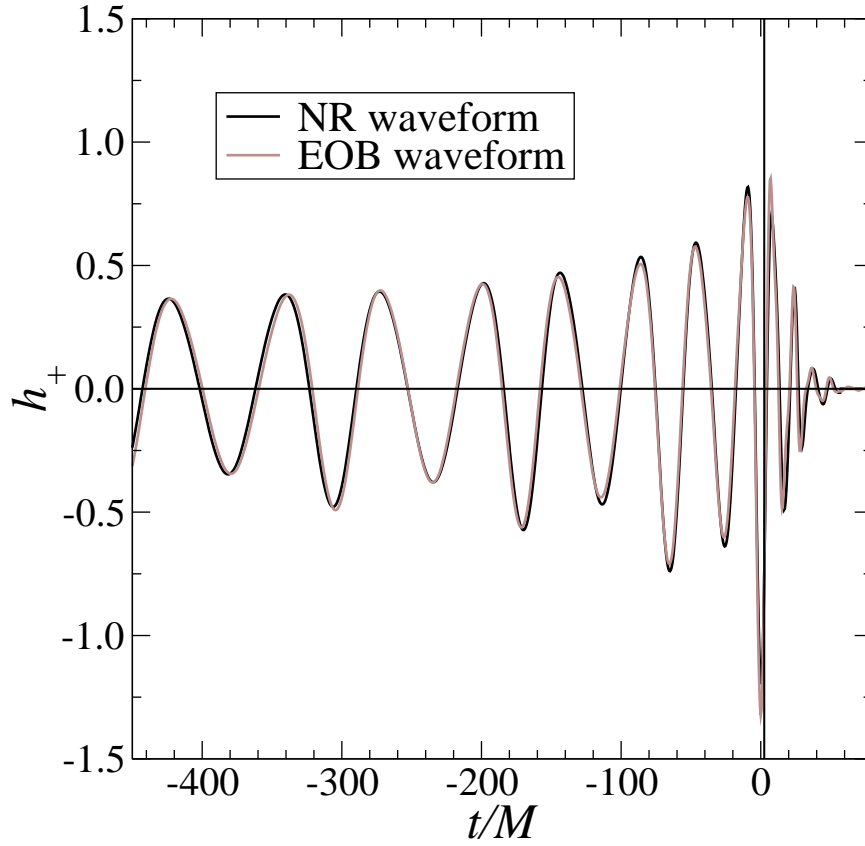


Figure 9: Comparison of merger waveforms for a $q = 4$ mass ratio non-spinning black hole binary calculated using the analytic “effective one-body” (EOB) model and using numerical relativity (NR). Reprinted with permission from (96) and copyright 2007 by the American Physical Society (<http://link.aps.org/abstract/PRD/v76/e104049>).